Control Mechanisms for Mobile Devices

Peter J. Smith[1], Ikram Singh[2], Pawel Dmochowski[2], Carl P. Dettmann[3] and Justin P. Coon[4]
[1] School of Mathematics and Statistics, Victoria University of Wellington, Wellington, NZ.
[2] School of Engineering and Computer Science, Victoria University of Wellington, Wellington, NZ.
[3] School of Mathematics, University of Bristol, Bristol, UK.
[4] Department of Engineering Science, University of Oxford, Oxford, UK.
{peter.smith,ikram.singh,pawel.dmochowski}@ecs.vuw.ac.nz, carl.dettmann@bris.ac.uk, justin.coon@eng.ox.ac.uk

***Abstract*—In this paper we consider control mechanisms for mobile devices in a stochastic environment. In particular, we consider a device in n-dimensional space subject to Brownian perturbations where a control mechanism moves the device towards its target location at a speed which is a function of its displacement. For this scenario, we construct stochastic differential equations for the mobility process and solve for the steady state probability density function of displacement. From this we are able to give general solutions to key metrics such as displacement outage (the long term probability of exceeding a given distance from the target), connectivity probability (derived from the SNR distribution in a Rayleigh channel with pathloss), the mean time at which the device first exceeds a given distance from the target, and the mean kinetic energy required by the control mechanism. We evaluate these metrics for important special cases of the control mechanism and also study the optimization problem of minimizing kinetic energy over the parameters of the control function.**

***Index Terms*– Mobile device, Brownian motion, kinetic energy, Fokker-Planck equation, stochastic differential equation, connectivity.**

I. Introduction

Autonomous devices are being proposed for applications in an increasing number of environments. These include ground-based robots [1]–[4], unmanned aerial vehicles (UAVs) [5]–[9] and nanobots [10]–[13]. For these applications, a fundamental requirement for further research is a model for the device mobility. There are two broad scenarios in which mobility models may be useful [14], [15]. In large scale applications, devices are deployed over hundreds of metres or kilometres. Here, the system designer may need mobility models to investigate connectivity issues or communication protocols between devices as the devices traverse a region. In high precision applications, small scale perturbations of the device are of interest. Note that two-dimensional (2D) models may be reasonable for some large scale applications where variation in altitude is much less than horizontal variation. However, 3D models are likely to be essential for many small scale applications. Hence, we consider n-dimensional models which can be specialised to physical 2D and 3D scenarios and also adapted to virtual multivariate mobility problems for vector processes.

In this area, the current stochastic mobility models [16]–[21] are overly simplistic, while mechanistic and chaotic models [22]–[25] tend to have no analytical possibilities. For example, simple stochastic models for position, such as Brownian motion (BM) [16] or the Ornstein-Uhlenbeck (OU) [26, p.106] process are physically unrealistic with jagged trajectories and strict constraints on covariance structure. Similarly, random waypoint models [17] produce simplistic trajectories unless complex variations are adopted. At the other extreme, complex models of device interactions and intelligence [27] lead to interesting mobility behaviour but analytical insights are rare. In [15] a more adaptable stochastic model has been proposed, but as with BM and the OU process, the model assumes linear control of position. Non-linear control was considered in [14] but only for the simplest on-off case where either a fixed velocity is applied in the desired direction or no control is applied. This motivates the work in this paper where we investigate stochastic mobility models which allow analytical results for non-linear controls.

To model both scenarios (large scale and small scale), we assume a centre or target position around which the devices move. Hence, we will model tethered devices. Extending the work to deterministic flight plans is straightforward. The models assume random fluctuations of position and a control function which controls the velocity in the desired direction as a function of displacement from the target. The generality achieved here is that any control velocity can be applied, extending the linear controls in [15]. The penalty paid for this generality is the assumption of symmetry in the n-dimensions which is needed to make analytical progress. Hence, the perturbations and controls in all dimensions are assumed to have the same statistics and the same form. With these assumptions we develop a set of coupled stochastic differential equations (SDEs) for position where the SDEs include random perturbations and an arbitrary control velocity.

From the underlying set of SDEs we obtain a single SDE for displacement from the target which is solved to give the steady state distribution of displacement and displacement moments. This fundamental derivation allows us to further study important features of the device mobility such as: precision (for small scale applications - how closely the device can maintain its position?); energy usage (how does the control function affect energy usage?); and connectivity (for large scale implementations - what are the statistics of device connectivity?). In particular, in this paper we make the following contributions:

- Precision is characterized by computing displacement outage probabilities (the probability of being further away

from the target than a given threshold) and MFHTs (the mean first hitting times at which the device first reaches a threshold distance from the target).

- Energy usage is characterized by evaluating the mean kinetic energy (KE) required by the different control functions. we also study the optimization problem of minimizing KE over the parameters of the control function.
- Connectivity is evaluated by the SNR outage probability for a link involving pathloss and Rayleigh fading.
- Analysis of all three areas described above is verified by simulation using three important families of control functions.

II. Mobility Model

Consider a device in n-dimensional space tethered to the origin and subject to independent BM perturbations in each of the n dimensions. A control mechanism moves the device towards its target (the origin) in the following manner. If $\mathbf{X}(t) = (X_1(t), X_2(t), \ldots, X_n(t))^T$ is the position of the device at time t then the control mechanism moves the device towards the target at velocity $v(R(t))$ where $v(\cdot)$ only depends on $R(t) = (X_1^2(t) + X_2^2(t) + \ldots + X_n^2(t))^{1/2}$, the radial displacement from the target. With this type of control, the velocity towards the origin in the i-th dimension is given by $v(R(t))X_i(t)/R(t)$. This allows us to describe the motion via a system of coupled SDEs.

A. SDEs

Extending the model in [14] to an arbitrary number of dimensions, the basic SDEs for position are given by

$$dX_i(t) = -\frac{v(R(t))X_i(t)}{R(t)}dt + \sigma dW_i(t), \quad \text{for} \quad i = 1, 2, \ldots, n,$$

where $W_i(t)$ are standard BM processes and σ^2 is the 'instantaneous variance' which controls the size of the perturbations. Writing the n SDEs in vector form gives:

$$d\mathbf{X}(t) = \mathbf{A}(\mathbf{X}(t))dt + \mathbf{B}d\mathbf{W}(t), \tag{1}$$

where $\mathbf{W}(t) = (W_1(t), W_2(t), \ldots, W_n(t))^T$, $\mathbf{A}(\mathbf{X}(t)) = (A_1(\mathbf{X}(t)), A_2(\mathbf{X}(t)), \ldots, A_n(\mathbf{X}(t)))^T$, $\mathbf{B} = \sigma^2\mathbf{I}_n$ and $A_i(\mathbf{X}(t)) = -v(R(t))X_i(t)/R(t)$.

Since the focus is on the displacement from the target rather than the actual position, we now convert the SDEs in (1) to a SDE for $R(t)$. This is achieved by the change of variable approach given in [26, Eq. 4.3.17]. Applying this to (1) gives:

$$dR(t) = \left(\sum_{i=1}^{n} A_i(\mathbf{X}(t))\partial_i R(t) + \frac{1}{2}\sum_{i,j=1}^{n}(\mathbf{B}\mathbf{B}^T)_{ij}\partial_i\partial_j R(t)\right)dt + \sum_{i,j=1}^{n}(\mathbf{B})_{ij}\partial_i R(t)dW_j(t), \tag{2}$$

where ∂_i represents the partial derivative, $\partial_i = \partial/\partial X_i(t)$. Noting that $\mathbf{B}$ is diagonal and directly computing the partial derivatives gives

$$dR(t) = \left(-\sum_{i=1}^{n}\frac{v(R(t))X_i^2(t)}{R^2(t)} + \frac{1}{2}\sum_{i=1}^{n}\sigma^2\left(\frac{1}{R(t)} - \frac{X_i^2(t)}{R^3(t)}\right)\right)dt + \sum_{i=1}^{n}\sigma\frac{X_i(t)}{R(t)}dW_i(t). \tag{3}$$

Using the definition $R^2(t) = \sum_{i=1}^{n} X_i^2(t)$ simplifies the drift coefficient in (3) giving

$$dR(t) = \left(-v(R(t)) + \frac{(n-1)\sigma^2}{2R(t)}\right)dt + \sum_{i=1}^{n}\sigma\frac{X_i(t)}{R(t)}dW_i(t). \tag{4}$$

Finally, from the properties of independent BM processes, we observe that the perturbation term, $\sum_{i=1}^{n}\sigma(X_i(t)/R(t))dW_i(t)$ is statistically identical to $\sigma dW(t)$ where $W(t)$ is another independent BM process. This follows from $\sum_{i=1}^{n} X_i^2(t)/R^2(t) = 1$. Hence, we obtain the final SDE

$$dR(t) = \left(-v(R(t)) + \frac{(n-1)\sigma^2}{2R(t)}\right)dt + \sigma dW(t). \tag{5}$$

B. Two-dimensional Example

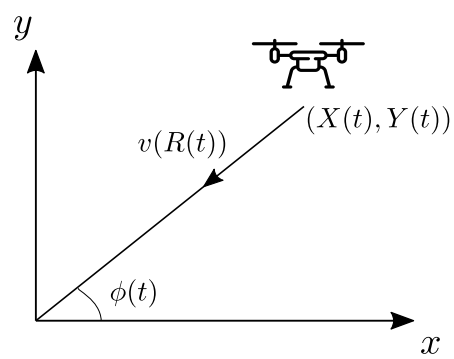

Fig. 1. Model diagram.

In this work, the main focus is on one to three dimensions where the process affords a visual representation and an example is useful for clarity. In Fig. 1, we show the special case of $n = 2$ and relabel the position $(X_1(t), X_2(t))$ in the traditional 2D notation as $(X(t), Y(t))$. The velocity, $v(R(t))$, is directed at the origin with angle $\phi(t)$ to the x-axis. This gives the SDEs

$$\left.\begin{aligned} dX(t) &= -v(R(t))\cos(\phi(t))dt + \sigma dW_1(t) \\ dY(t) &= -v(R(t))\sin(\phi(t))dt + \sigma dW_2(t). \end{aligned}\right\} \tag{6}$$

Noting that $\cos(\phi(t)) = X(t)/R(t)$ and $\sin(\phi(t)) = Y(t)/R(t)$ we immediately see how the SDEs in (6) collapse to (1).

C. Steady State Displacement Distribution

Associated with the SDE in (5) is the Fokker-Planck differential equation for the PDF, $f(x,t)$, which is the PDF of $R(t)$ evaluated at x. From [26, p.234], this is given by

$$\frac{\partial f(x,t)}{\partial t} = -\frac{\partial}{\partial x}\left(\left(-v(x) + \frac{(n-1)\sigma^2}{2x}\right) f(x,t)\right) + \frac{\sigma^2}{2}\frac{\partial^2 f(x,t)}{\partial x^2}. \quad (7)$$

The steady state solution of (7), if it exists, is found by setting $\frac{\partial f(x,t)}{\partial t} = 0$ and $f(x,t) = f(x)$, where $f(x)$ is the PDF of R (the steady state displacement). This leads to the first order differential equation

$$\left(-v(x) + \frac{(n-1)\sigma^2}{2x}\right) f(x) = \frac{\sigma^2}{2}\frac{df(x)}{dx}. \quad (8)$$

This is easily solved by integrating factor methods, giving the solution

$$f(x) = Kx^{n-1}\exp\left(-\frac{2V(x)}{\sigma^2}\right), \quad (9)$$

where $V(x) = \int_0^x v(\tau)d\tau$ and K is a normalizing constant so that $\int_0^\infty f(x)dx = 1$. Hence, the steady state PDF of displacement is available for all control mechanisms which allow a solution. Displacement 'outage' probabilities can therefore be obtained via

$$P(R > R_D) = \int_{x=R_D}^{\infty} Kx^{n-1}\exp\left(-\frac{2V(x)}{\sigma^2}\right)dx. \quad (10)$$

For reasonable control functions, $v(x)$, which are likely to be envisaged, it is probable that $V(x)$ can be obtained in closed form so that (9) provides a closed form displacement PDF. However, $V(x)$ occurs in the exponent in (10) making the integration more challenging. For most control functions beyond piecewise linear, it is likely that evaluation of the outage probabilities in (10) requires a single numerical integration.

From (9), the steady state moments of displacement are obtained as

$$E[R^k] = \int_0^\infty Kx^{n+k-1}\exp\left(-\frac{2V(x)}{\sigma^2}\right)dx. \quad (11)$$

D. Large Displacement Probability

An important class of velocity functions are those which are monotonically increasing and have a ceiling such that $v(R(t)) \to c$ as $R(t) \to \infty$. The monotonicity arises from the logic that there is more need to move towards the target at larger displacements so the velocity would be increased or held constant, but not reduced. The ceiling arises from practical upper limits on device velocity. For such velocity functions and large displacements, R_D, we can write $v(R_D) = c - \Delta$ where $\Delta > 0$ is small. We can also bound the values of $V(x)$ in $x \geq R_D$ by

$$V(x) \geq V(R_D) + (x - R_D)(c - \Delta) \triangleq a + bx. \quad (12)$$

Substituting (12) into (10) gives

$$P(R > R_D) \leq \int_{x=R_D}^{\infty} Kx^{n-1}\exp\left(-\frac{2(a+bx)}{\sigma^2}\right)dx = K\exp\left(-\frac{2a}{\sigma^2}\right)\left(\frac{\sigma^2}{2b}\right)^n \Gamma\left(n, \frac{2bR_D}{\sigma^2}\right), \quad (13)$$

where $\Gamma(\cdot,\cdot)$ is the upper incomplete gamma function, $a = V(R_D) - R_D(c - \Delta)$ and $b = c - \Delta$. While (13) provides an upper bound, an even simpler approximation can also be constructed. First, we use the approximation $V(x) \approx V(R_D) + (x - R_D)c$ in (10) followed by the asymptotic result, $\Gamma(r,s) \sim s^{r-1}\exp(-s)$ for large s [28]. This gives the approximate result

$$P(R > R_D) \approx K\left(\frac{\sigma^2}{2c}\right)R_D^{n-1}\exp\left(-\frac{2V(R_D)}{\sigma^2}\right). \quad (14)$$

E. Connectivity Probability

Consider the mobile device communicating with a fixed device at the origin. The classical model for the SNR of this link involving pathloss and Rayleigh fading is given by

$$\gamma(t) = AR(t)^{-\eta}|h(t)|^2, \quad (15)$$

where A is a constant, $R(t)$ is displacement, η is the pathloss exponent and $h(t)$ is the fast fading normalized Rayleigh channel gain with $E[|h(t)|^2] = 1$. We assume that connectivity occurs above a certain SNR threshold, γ_C. In steady state the connectivity probability is therefore

$$\begin{aligned} P(\gamma(t) > \gamma_C) &= E[P(|h(t)|^2 > \gamma_C R^\eta/A|R)] \\ &= E[\exp(-\gamma_C R^\eta/A)] \\ &= \int_{x=0}^{\infty} Kx^{n-1}\exp\left(-\frac{2V(x)}{\sigma^2} - \frac{\gamma_C x^\eta}{A}\right)dx, \end{aligned} \quad (16)$$

using the fact that $|h(t)|^2$ is exponential and substituting the PDF of displacement, $f(x)$, given in (9). For piecewise linear control functions and $\eta = 2$, (16) is tractable and closed form connectivity probabilities are available. For most other cases, (16) gives a general solution requiring a single numerical integration.

F. Mean First Hitting Time

In order to derive the MFHT, we first express the underlying FPE in (7) in a more general form as:

$$\frac{\partial f(x,t)}{\partial t} = -\frac{\partial}{\partial x}\left(A(x)f(x,t)\right) + \frac{1}{2}\frac{\partial^2(B(x)f(x,t))}{\partial x^2}. \quad (17)$$

In our case, $A(x) = -v(x) + (n-1)\sigma^2/(2x)$ and $B(x) = \sigma^2$. From [26, p.234], the MFHT of an object located at $x = a$ at $t = 0$ hitting a boundary $b > a$ is given by $T_{a,b}$, where

$$T_{a,b} = 2\int_{y=a}^{b}\frac{1}{\psi(y)}\int_{z=a}^{y}\frac{\psi(z)}{B(z)}dzdy, \quad (18)$$

and

$$\psi(u) = \exp\left(\int_{x=a}^{u} \frac{2A(x)}{B(x)} dx\right). \tag{19}$$

For our case, substituting $A(x)$, $B(x)$ and $a = 0$ into (19) and (18) gives:

$$T_{0,b} = \frac{2}{\sigma^2} \int_0^b \int_0^y \left(\frac{z}{y}\right)^{n-1} \exp\left(\frac{2(V(y) - V(z))}{\sigma^2}\right) dz dy. \tag{20}$$

For piecewise linear control functions, the inner integral in (20) is tractable, but numerical integration is almost always required for the outer integral.

G. Kinetic Energy

In steady state, the mean kinetic energy provided by the control mechanism is $\mu_{KE} = E[m_0 v^2(R)/2]$ where m_0 is the mass of the device and R is the steady state displacement. Using (9) we obtain:

$$\mu_{KE} = \frac{m_0}{2} \int_0^\infty v(x)^2 K x^{n-1} \exp\left(-\frac{2V(x)}{\sigma^2}\right) dx. \tag{21}$$

For piecewise linear control functions, (21) is tractable and closed form kinetic energies are available. For most other cases, (21) gives a general solution requiring a single numerical integration.

III. Special cases

The best known special case is the two-dimensional OU process where $v(x) = \alpha x$ for some positive constant, α. In this case, the processes, $X_1(t)$, $X_2(t)$ $R(t)$ are well known, see for example [26, p.234] and [29], and extensive transient as well as steady state results are available since, in this case, $X_1(t)$, $X_2(t)$ are Gaussian. In most other cases the transient solution is not available but steady state results on the displacement PDF, connectivity probability, MFHT and kinetic energy are given in Secs. II-C, II-E, II-F and II-G. It is reasonable that a control mechanism would apply a velocity, $v(x)$, which is an increasing function of displacement. However, a linear $v(x)$ function is simplistic and does not model physical features such as a maximum velocity or threshold control where the device is only moved if its displacement exceeds a certain value. Hence, we consider three special cases: 'on-off' control (OC), ramp control (RC) and sigmoid control (SC) which cover these important features. The control functions are given below. For OC,

$$v_{OC}(x) = \begin{cases} 0 & \text{if } x \le m \\ c & \text{if } x > m, \end{cases} \tag{22}$$

where c is the maximum velocity and m is the threshold. The corresponding expression for $V_{OC}(\cdot)$ is

$$V_{OC}(x) = \begin{cases} 0 & \text{if } x \le m \\ (x-m)c & \text{if } x > m. \end{cases} \tag{23}$$

For RC,

$$v_{RC}(x) = \begin{cases} 0 & \text{if } x \le \max(0, m-s) \\ c(x-m+s)/s & \text{if } \max(0, m-s) < x \le m \\ c & \text{if } x > m, \end{cases} \tag{24}$$

where c is the maximum velocity, m is the threshold at which maximum velocity is applied and $m - s$, where $s > 0$, is the start point of the ramp. Defining $L = \max(0, m - s)$, the corresponding expression for $V_{RC}(\cdot)$ split into the same 3 regions as in (24) is

$$V_{RC}(x) = \begin{cases} 0 \\ \frac{c}{2s}(x^2 - L^2 - 2(m-s)(x-L)) \\ V_{RC}(m) + (x-m)c. \end{cases} \tag{25}$$

Finally, for SC,

$$v_{SC}(x) = \begin{cases} 0 & \text{if } x \le 0 \\ c/(1 + \exp(-(x-m)/s) & \text{if } x > 0, \end{cases} \tag{26}$$

where c is the maximum velocity, m is the mid-point and $1/s$ is the growth rate of the sigmoid. The corresponding expression for $V_{SC}(\cdot)$ is

$$V_{SC}(x) = \begin{cases} 0 & \text{if } x \le 0 \\ cs\log(1 + \exp((x-m)/s) & \text{if } x >, 0 \end{cases} \tag{27}$$

In all three scenarios, c is maximum velocity and m locates the function. For RC and SC, s is a measure of steepness.

Since $v_{OC}(x)$ and $v_{RC}(x)$ are piecewise linear, closed form results are available for the displacement PDF leading to displacement outage, connectivity probability and kinetic energy. For OC, the MFHT is also available in closed form. For SC, results are obtained via numeric integrations.

A. Ramp Control (RC) and On-Off Control (OC)

In this section, we focus on the derivations for RC. Since the most complex form of $V_{RC}(x)$ is a quadratic in x, while $V_{OC}(x)$ is only linear in x, we can obtain OC results as a special case of RC. Substituting (25) into (10) requires three types of integrals, The first is $\int_a^\infty x^m \exp(-bx)dx$ given in [30, Eq. 3.351.2] and the second is $\int_0^a x^2 \exp(-bx^2)dx$ given in [30, Eq. 3.381.8] as an incomplete gamma function, which also has a representation in terms of the error function, erf$(\cdot)$. For both integrals, $a > 0$, $b > 0$ and m is a positive integer. The third integral is $I_m = \int_a^\infty x^m \exp(-bx^2 - cx)dx$ for $c > 0$ and $m \in \{2, 3, 4\}$. Expanding I_m gives

$$I_m = \frac{1}{2b} \int_a^\infty x^{m-1} ((2bx + c) - c) \exp(-bx^2 - cx) dx. \tag{28}$$

Now, using integration by parts, I_m can be written as

$$I_m = \frac{1}{2b} \left(-cI_{m-1} + (m-1)I_{m-2} + a^{m-1} \exp(-ba^2 - ca)\right). \tag{29}$$

Hence, using the recursion in (29), I_m can be solved in terms of I_0 which is given in [30, Eq. 3.322.1].

Due to the number of possible cases (OC, RC, SC in 2D or 3D), in the numerical results section, we focus on 3D results and for the RC case, only the $m > s$ case is shown. Hence, we only show the mathematical expressions for these scenarios. All other cases can be derived using the methodology above.

For RC, substituting the three integral results into K and (10), (16), (21) gives the results in (37)-(41), in the Appendix, where $\gamma(\cdot,\cdot)$ is the lower incomplete gamma function and $E_1(\cdot)$ is the exponential integral.

In the same way, for OC, substituting the three integral results into K and (10), (16), (20), (21) gives the results in (31)-(34) in the Appendix, where $\text{erfc}(\cdot)$ is the complementary error function.

IV. Optimal Control

The control mechanism will ideally maintain the device close to the origin with little expenditure of energy. Proximity to the origin could be measured in several ways. For example, via a target connectivity probability, P_C, such that $P(\gamma(t) > \gamma_C) \geq P_C$, a target displacement, R_D, with associated probability, P_D, such that $P(R > R_D) \leq P_D$ or a target MFHT, T_{MFHT}, such that $T_{0,R_D} > T_{\text{MFHT}}$. Here, we focus on obtaining an acceptably low probability of excursions beyond R_D in steady state. Minimizing the kinetic energy requires the minimization of (21) over the parameters of the control function. Here, we focus on the three special cases in Sec. III so that the mean kinetic energy is labelled $\mu_{KE}(m,s,c)$, with some abuse of notation as the s parameter is not present in OC. Hence, in this paper, we focus on the optimization problem,

$$(m^*, s^*, c^*) = \underset{m,s,c}{\text{argmax}} \; -\mu_{KE}(m,s,c) \quad \text{such that} \quad P(R > R_D) \leq P_D. \tag{30}$$

For OC and RC, closed form expressions are given in Sec. III for μ_{KE} and $P(R > R_D)$. For SC, these expressions are obtained via numeric integration of (21) and (10). The minimization in (30) is performed by an interior point algorithm and results are shown in Sec. V.

A second optimization problem considered is to maximize the connectivity probability with a limited kinetic energy budget. Hence, using the same framework as above, we obtain the problem,

$$(m^*, s^*, c^*) = \underset{m,s,c}{\text{argmax}} \; P(\gamma(t) > \gamma_C) \quad \text{such that} \quad \mu_{KE}(m,s,c) \leq \mu_0. \tag{31}$$

For OC and RC, closed form expressions are given in Sec. III for μ_{KE}. For SC, the expression is obtained via numeric integration of (21). Connectivity probabilities are obtained using (16). The minimization in (31) is performed by an interior point algorithm and results are shown in Sec. V.

V. Numerical results

In this section, we first verify the analytical results for distance outage probability, connectivity probability and MFHT. For outage probability and MFHT we consider 3D scenarios and for connectivity we assume a 2D situation which models the case where the vertical spread is much smaller than the azimuthal variation. Unless otherwise specified, the numerical values of parameters used are given in Table I

Control Type	Parameter	Value
all	c	5
	σ^2	1
	A	2
	m_0	1
	η	2
OC	m	2.1
RC	m_{RCnarrow}, m_{RCbroad}	2.52, 3.15
	s_{RCnarrow}, s_{RCbroad}	0.84, 2.1
SC	m_{SCnarrow}, m_{SCbroad}	2.1, 2.1
	s_{SCnarrow}, s_{SCbroad}	1/5, 1/2.1

TABLE I
Parameter values used in Figs. 2-5.

In Fig. 2, we plot the outage probability, $P(R > R_D)$ vs R_D for all 5 scenarios (narrow and broad RC, narrow and broad SC and OC). The analysis agrees with the simulations in all cases. The fundamental trend in Fig. 2 is that narrower control functions give higher outage probabilities. Note that all the control functions are centred on the same value so the key parameter distinguishing them is the spread parameter. Hence, OC has the highest outage, followed by RC (narrow), SC (narrow), RC (broad) and lastly, SC (broad) which has the lowest outage. This is because the broader functions begin to operate earlier and exert more control over small displacements. Analytical results are computed using (32), (33) for OC, (38), (39), (40) for RC (both in the Appendix) and (10) for SC.

In Fig. 3, we plot the connectivity probability vs the threshold, γ_C, for the same five scenarios given in Fig. 2. All analytical results are supported by simulations. We observe that the order of performance is exactly the same as in Fig. 2, where OC is worst and SC (broad) is best. Again, the reason for the trend is the extra control provided by the broader control functions which begin to operate at smaller displacements than the narrower control functions. Analytical results are computed using (42) for OC, (43) for RC and (16) for SC.

In Fig. 4, we plot the MFHT, $T_{0,b}$, vs the threshold, b, for the same five scenarios given in Fig. 2. All analytical results are supported by simulations. The MFHT results are not very sensitive to the type of control function for small thresholds but diverge at higher values. The effect for the higher values is that the control functions which reach maximum effect first are more effective at slowing down excursions to the threshold. Hence, OC has the longest MFHT followed by RC (narrow) and RC (broad). In contrast, SC is smooth and only approaches the peak value of c, so that the MFHT values for SC are smaller with SC (broad) the smallest MFHT. Analytical results are computed using (35), (36) for OC and (20) for RC and

SC.

In Fig. 5, we plot the outage probability, $P(R > R_D)$ vs R_D for 3 scenarios (narrow RC, broad SC and OC). The outage probabilities are on a log-scale to highlight the accuracy of the simple large displacement approximations. Analytical results are computed as in Fig. 2 for exact results and using (14) for the approximations. The approximations agree very well with the exact results in all cases where the outage probability is small (say less than 10^{-2}).

In Fig. 6, we plot the optimal (minimum) mean kinetic energy vs R_D for a fixed target probability, $P_D = 0.1$. As expected, RC and SC deliver lower KE values as they control mobility at smaller distances than OC, hence reducing the need for the maximal control velocity. However, the gap between OC and RC/SC is not large. Results for SC and RC are visually indistinguishable.

In order to see how the three different control mechanisms minimize the mean KE we plot the optimal control functions for $R_D = 0.1$ in Fig. 7. We observe that the basic position of all three functions is similar and the slopes of v_{RC} and v_{SC} are similar. Hence, the different functions operate by trading off low displacement control for maximum velocity. At small displacements, SC has the most control, followed by RC and then OC. Hence, SC usually avoids larger displacements and can therefore have a higher maximum velocity without inflating the KE. At the other extreme, OC has no control at low displacements. This causes larger displacements and therefore the maximum velocity is reduced to avoid increasing the KE.

In Fig. 8, we observe the maximum connectivity probability according to a varying upper bound on kinetic energy, μ_0, and a particular set of γ_C values. The basic trends are as expected: connectivity improves with more energy and connectivity improves as γ_C decreases. The relative values given by OC, RC and SC are of more interest. As in Fig. 7 the results for OC are worse than for RC and SC which are indistinguishable. In the upper and lower tails all three control types are very similar, with the largest differences being in the centre where differences of a few percent can be observed. The small variation between control types is reasonable as connectivity is a large-scale issue unlikely to be strongly affected by local variations in control.

VI. Conclusions

We have developed a tractable SDE model for mobility extending prior work to handle arbitrary non-linear controls. The models cater for n-dimensions so that physical mobility scenarios (2D and 3D) as well as vector processes may be considered. The SDEs deliver simple integral expressions for important performance metrics such as distance outage, MFHT, connectivity probability and mean KE. For typical examples of non-linear control functions, we obtain analytical expressions for these metrics and identify the following insights into the effect of the control function on performance. For control functions *located* in the same place, broader control functions are usually beneficial. Since the broader functions apply more control at smaller displacements, they tend to reduce deviations from the target and improve distance outage, connectivity and reduce KE. However, for large excursions from the target, narrower control helps the MFHT as this introduces maximum control earlier, making it harder to attain larger displacements. These conclusions are all in the context of monotonic increasing control functions with a ceiling.

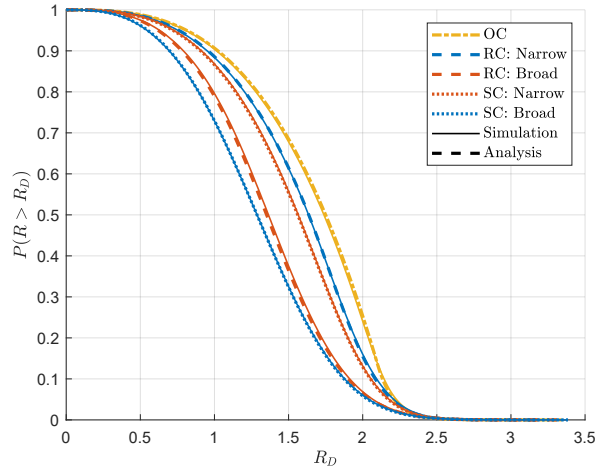

Fig. 2. Outage probability, $P(R > R_D)$, vs R_D.

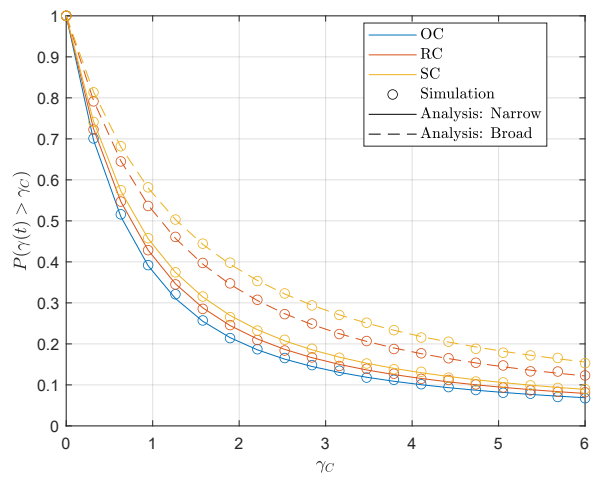

Fig. 3. Connectivity probability, $P(\gamma(t) > \gamma_C)$, vs γ_C.

References

[1] T. Balch and R. Arkin, "Behavior-based formation control for multirobot teams," *IEEE Trans. Robot. Autom.*, vol. 14, no. 6, pp. 926–939, 1998.

[2] Y. Cao, A. Fukunaga, and A. Kahng, "Cooperative mobile robotics: Antecedents and directions," *Autonomous Robots*, vol. 4, no. 1, pp. 7–27, 1997.

[3] Z. Yan, N. Jouandeau, and A. A. Cherif, "A survey and analysis of multi-robot coordination," *Intern. J. Advanced Robotic Systems*, vol. 10, no. 12, p. 399, 2013.

[4] Y. Rizka, M. Awad, and E. Tunstel, "Cooperative heterogeneous multi-robot systems: A survey," *ACM Computing Surveys (CSUR)*, vol. 52, no. 2, pp. 1–31, 2019.

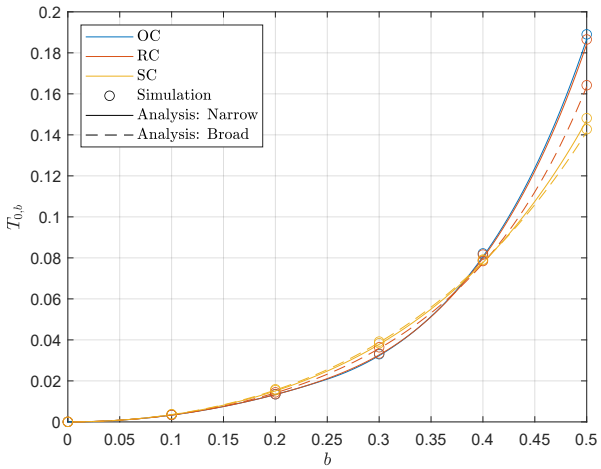

Fig. 4. MFHT, $T_{0,b}$, vs b.

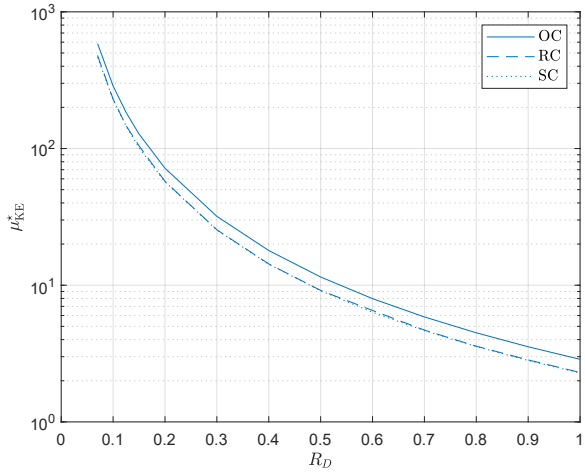

Fig. 6. Minimum mean KE vs R_D with $P_D = 0.1$.

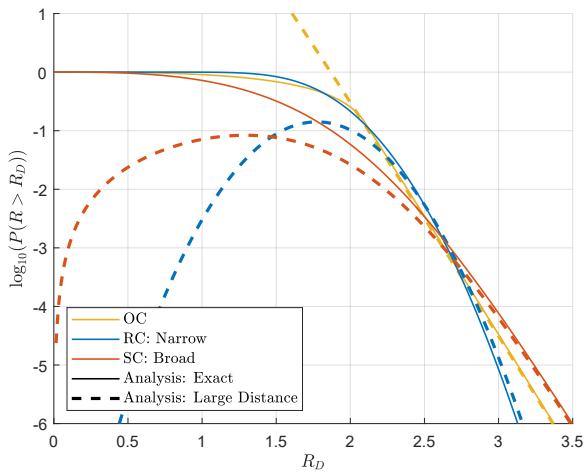

Fig. 5. Outage probability, $P(R > R_D)$, vs R_D with large distance approximations.

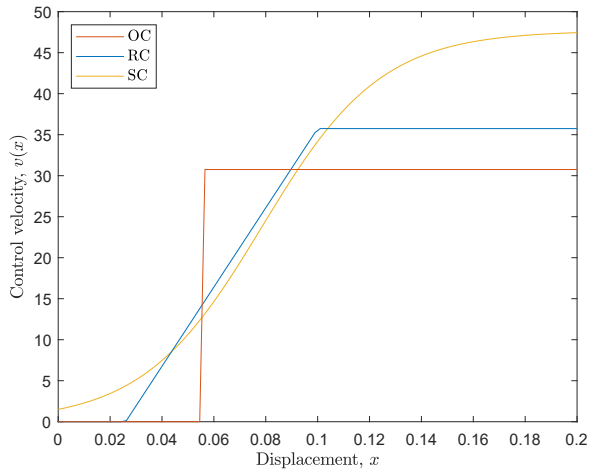

Fig. 7. Control velocity vs displacement.

[5] M. Campion *et al.*, "A review and future directions of UAV swarm communication architectures," in *IEEE Intern. Conf. on Electro/Inf. Technol. (EIT)*, 2018, pp. 0903–0908.

[6] ——, "UAV swarm communication and control architectures: A review," *J. Unmanned Vehicle Systems*, vol. 7, no. 2, pp. 93–106, 2018.

[7] E. Kalantari, H. Yanikomeroglu *et al.*, "On the number and 3D placement of drone base stations in wireless cellular networks," in *Proc. of IEEE Veh. Technol. Conf.*, 2016.

[8] R. Palat, A. Annamalau, and J. Reed, "Cooperative relaying for ad-hoc ground networks using swarm UAVs," in *Proc. IEEE Military Commun. Conf. (MILCOM)*, Oct. 2005, pp. 1588–1594 Vol. 3.

[9] I. Bor-Yaliniz and H. Yanikomeroglu, "The new frontier in RAN heterogeneity: Multi-tier drone-cells," *IEEE Commun. Mag.*, vol. 54, no. 11, pp. 48–55, Nov. 2016.

[10] S. Dolev, R. Narayanan, and M. Rosenblit, "Design of nanorobots for exposing cancer cells," *Nanotechnology*, vol. 30, no. 31, p. 315501, 2019.

[11] V. Loscri and A. Vegni, "An acoustic communication technique of nanorobot swarms for nanomedicine applications," *IEEE Trans. Nanobiosci.*, vol. 14, no. 6, pp. 598–607, 2015.

[12] G. Cerofolini, P. Amato, M. Masserini, and G. Mauri, "A surveillance system for early-stage diagnosis of endogenous diseases by swarms of nanobots," *Advanced Science Letters*, vol. 3, no. 4, pp. 345–352, 2010.

[13] Y. Chen, P. Anwar, L. Huang, and M. Asvial, "Characterizing nanoscale transient communication," *IEEE Trans. Nanobiosci.*, vol. 15, no. 3, pp. 218–229, Apr. 2016.

[14] P. J. Smith, P. A. Dmochowski, I. Singh, R. Green, C. P. Dettmann, and J. P. Coon, "3D mobility models and analysis for UAVs," in *Proc IEEE International Symposium on Personal, Indoor and Mobile Radio Communications (PIMRC)*, Sep. 2020.

[15] P. J. Smith, I. Singh, P. A. Dmochowski, J. P. Coon, and R. Green, "Flexible mobility models using stochastic differential equations," *IEEE Trans. Veh. Technol.*, 2021, under review.

[16] T. Camp, J. Boleng, and V. Davies, "A survey of mobility models for ad hoc network research," *Wireless Commun. and Mobile Comput.*, vol. 2, no. 5, pp. 483–502, 2002.

[17] C. Bettstetter, G. Resta, and P. Santi, "The node distribution of the random waypoint mobility model for wireless ad hoc networks," *IEEE Trans. Mobile Comput.*, vol. 2, no. 3, pp. 257–269, 2003.

[18] P. Sharma *et al.*, "Random 3D mobile UAV networks: Mobility modeling and coverage probability," *IEEE Trans. Wireless Commun.*, vol. 18, no. 5, pp. 2527–2538, May 2019.

[19] P. Nain *et al.*, "Properties of random direction models," in *Proc. Annual Joint Conf. of IEEE Computer and Commun. Societies.*, vol. 3, 2005, pp. 1897–1907.

[20] B. Liang and Z. Haas, "Predictive distance-based mobility management for multidimensional PCS networks," *IEEE/ACM Trans. Netw.*, vol. 11, no. 5, pp. 718–732, Oct. 2003.

[21] M. Banagar, V. V. Chetlur, and H. S. Dhillon, *Stochastic Geometry-*

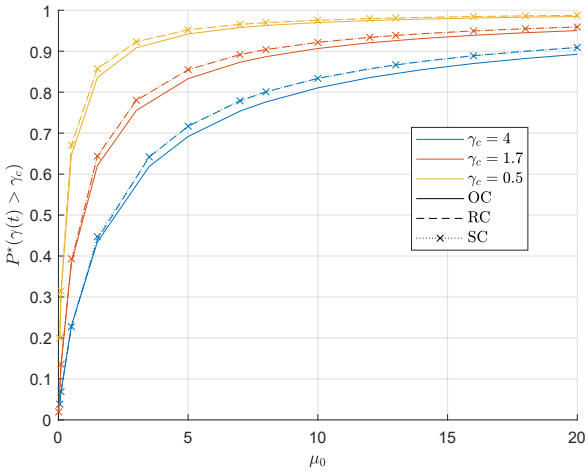

Fig. 8. Maximum connectivity probability vs μ_0 for $\gamma_C \in \{0.5, 1.7, 4\}$.

Based Performance Analysis of Drone Cellular Networks. John Wiley & Sons, Ltd, 2020, ch. 9, pp. 231–254.

[22] J. Dentler *et al.*, "Collision avoidance effects on the mobility of a UAV swarm using chaotic ant colony with model predictive control," *J. Intelligent and Robotic Systems*, vol. 93, no. 1-2, pp. 227–243, 2019.

[23] M. Rosalie *et al.*, "From random process to chaotic behavior in swarms of UAVs," in *Proc. 6th ACM Symp. on Dev. and Analysis of Intell. Veh. Netw. and Applications*. ACM, 2016, pp. 9–15.

[24] ——, "Chaos-enhanced mobility models for multilevel swarms of UAVs," *Swarm and Evolutionary Computation*, vol. 41, pp. 36–48, 2018.

[25] D. H. Stolfi, M. R. Brust, G. Danoy, and P. Bouvry, "A cooperative coevolutionary approach to maximise surveillance coverage of uav swarms," in *2020 IEEE 17th Annual Consumer Communications and Networking Conference (CCNC)*. IEEE, 2020, pp. 1–6.

[26] C. W. Gardiner, *Stochastic Methods: A Handbook for the Natural and Social Sciences*. Springer-Verlag, 2009.

[27] W. Wang, J. Wang, M. Wang, B. Wang, and W. Zhang, "A realistic mobility model with irregular obstacle constraints for mobile ad hoc networks," *Wireless Networks*, vol. 25, no. 2, pp. 487–506, 2019.

[28] M. Abramowitz and I. A. Stegun, *Handbook of Mathematical Functions with Formulas, Graphs, and Mathematical Tables*. US Government Printing Office, 1964, vol. 55.

[29] P. Smith and J. Coon, "Connectivity times for mobile D2D networks," in *2018 IEEE International Conference on Communications (ICC)*, 2018, pp. 1–6.

[30] I. S. Gradshteyn and I. M. Ryzhik, *Table of Integrals, Series, and Products*. Elsevier Inc., 2007.

APPENDIX

Here we provide 3D and 3D results for OC and RC control scenarios.

3D OC Results: For ease of notation, let $\beta = \frac{c}{\sigma^2}$, then

$$K^{-1} = \frac{m^3}{3} + \frac{2m\beta(m\beta+1)+1}{4\beta^3} \tag{31}$$

$$P(R > R_D) = 1 - \frac{K}{3}R_D^3 \quad \text{for} \quad R_D \leq m \tag{32}$$

$$P(R > R_D) = 1 - \frac{Km^3}{3} - \frac{2K\beta(m(m\beta+1) + R_D(R_D\beta+1)\exp(2\beta(m-R_D)))}{4\beta^3} \quad \text{for} \quad R_D > m \tag{33}$$

$$\mu_{\text{KE}} = \frac{m_0 K c^2(2m(m\beta+1)+1)}{8\beta^3} \tag{34}$$

$$T_{0,b} = \frac{b^2}{3\sigma^2} \quad \text{for } b < m \tag{35}$$

$$\begin{aligned} T_{0,b} = &\frac{m^2}{3\sigma^2} + \frac{m-b}{c} + \frac{1}{c\beta}\ln\left\{\frac{m}{b}\right\} + \frac{1}{2c\beta^2}\left(\frac{1}{b} - \frac{1}{m}\right) \\ &+ e^{-2m\beta}\left(\frac{2m^3}{3\sigma^2} + \frac{1}{2c\beta^2} + \frac{m^2}{c} + \frac{m}{c\beta}\right)\left(\frac{e^{2m\beta}}{m} - \frac{e^{2b\beta}}{b} + 2\beta\left(E_1(-2m\beta) - E_1(-2b\beta)\right)\right) \quad \text{for } b \geq m \end{aligned} \tag{36}$$

3D RC results for $m > s$: For ease of notation, let $\beta = \frac{c}{\sigma^2}, R_1 = m - s$, then

$$K^{-1} = \frac{R_1^3}{3} + \frac{s^{3/2}\gamma\left(\frac{3}{2}, s\beta\right)}{2\beta^{3/2}} + \frac{sR_1\gamma\left(1, s\beta\right)}{2\beta} + \frac{\sqrt{s\pi}R_1^2}{2\sqrt{\beta}}\text{erf}\left(\sqrt{s\beta}\right) + \frac{e^{\beta(2m-s)}\Gamma\left(3, 2m\beta\right)}{8\beta^3} \tag{37}$$

$$P(R > R_D) = 1 - \frac{K}{3}R_D^3 \quad \text{for} \quad R_D \leq m - s \tag{38}$$

$$\begin{aligned} P(R > R_D) = 1 - &\frac{KR_1^3}{3} - \frac{s^{3/2}K\gamma\left(\frac{3}{2}, \frac{\beta(R_D-R_1)^2}{s}\right)}{2\beta^{3/2}} - \frac{sKR_1\gamma\left(1, \frac{\beta(R_D-R_1)^2}{s}\right)}{\beta} \\ &- \frac{KR_1^2\sqrt{s\pi}}{2\sqrt{\beta}}\text{erf}\left(\frac{\sqrt{\beta}(R_D - R_1)}{\sqrt{s}}\right) \quad \text{for} \quad m - s < R_D \leq m \end{aligned} \tag{39}$$

$$\begin{aligned} P(R > R_D) = 1 - &\frac{KR_1^3}{3} - \frac{s^{3/2}K\gamma\left(\frac{3}{2}, s\beta\right)}{2\beta^{3/2}} - \frac{sKR_1\gamma\left(1, s\beta\right)}{\beta} - \frac{KR_1^2\sqrt{s\pi}}{2\sqrt{\beta}}\text{erf}\left(\sqrt{s\beta}\right) \\ &- \frac{Ke^{\beta(2m-s)}}{8\beta^3}\left(\Gamma\left(3, 2m\beta\right) - \Gamma\left(3, 2R_D\beta\right)\right) \quad \text{for} \quad R_D > m \end{aligned} \tag{40}$$

$$\mu_{KE} = \frac{m_0 K}{2}\left(\frac{c^2}{s^2}\left(\frac{s^{5/2}\gamma\left(\frac{5}{2}, s\beta\right)}{2\beta^{5/2}} + \frac{2s^2R_1\gamma\left(2, s\beta\right)}{2\beta^2} + \frac{s^{3/2}R_1^2\gamma\left(\frac{3}{2}, s\beta\right)}{2\beta^{3/2}}\right) + \frac{c^2e^{\beta(2m-s)}\Gamma\left(3, 2m\beta\right)}{8\beta^3}\right) \tag{41}$$

2D OC Connectivity: For ease of notation, let $g = \frac{\gamma_C}{A}, b = -\frac{\beta A}{\gamma_C}$

$$P(\gamma(t) > \gamma_C) = \frac{K(1 - e^{-gm^2})}{2g} + Ke^{2\beta m + gb^2}\left(\frac{e^{-g(m-b)^2}}{2g} + \frac{b\sqrt{\pi}}{2\sqrt{g}}\text{erfc}(\sqrt{g}(m-b))\right) \tag{42}$$

2D RC Connectivity when $m > s$: For ease of notation, let $g = \frac{\gamma_C}{A}, b = -\frac{\beta A}{\gamma_C}, R_2 = \frac{\beta}{s} + g, R_3 = \frac{\beta R_1}{sR_2}$

$$\begin{aligned} P(\gamma(t) > \gamma_C) = &\frac{K(1 - e^{-gR_1^2})}{2g} + Ke^{\beta(2m-s)+gR_3^2}\left[\frac{e^{-g(m-b)^2}}{2g} + \frac{b\sqrt{\pi}}{2\sqrt{g}}\text{erfc}(\sqrt{g}(m-b))\right] \\ &+ Ke^{-\frac{\beta R_2^2}{s}+R_2R_3^2}\left[\frac{e^{-R_2(R_1-R_3)^2} - e^{-R_2(m-R_3)^2}}{2R_2} + \frac{R_3\sqrt{\pi}}{2R_2}\left(\text{erfc}(\sqrt{R_2}(R_1-R_3)) - \text{erfc}(\sqrt{R_2}(m-R_3))\right)\right] \end{aligned} \tag{43}$$